World Conference on
Timber Engineering
Oslo 2023

# CYCLIC TESTING AND NUMERICAL MODELING OF A THREE-STORY MASS-TIMBER BUILDING WITH A PIVOTING MASS PLY PANEL SPINE AND BUCKLING-RESTRAINED ENERGY DISSIPATORS

**Gustavo A. Araujo R.[1], Barbara G. Simpson[2], Tu X. Ho[3], Gustavo F. Orozco O.[4], Andre R. Barbosa[5], and Arijit Sinha[6]**

**ABSTRACT:** Mass timber panels are emerging as an innovative alternative for the design of elastic spines due to their high stiffness- and strength-to-weight ratio, among other factors. Recent research has shown that mass timber panels used in conjunction with steel energy dissipators are promising solutions for enhanced seismic performance. However, the available experimental data at the building scale is still minimal, which limits the understanding, adoption, and development of effective seismic design guidelines for these systems. This research addresses this gap through full-scale quasi-static cyclic testing of a three-story mass timber building. Lateral loads are transferred through Mass Ply Panel (MPP) diaphragms to an MPP spine with vertically-oriented unbonded steel buckling-restrained braces (BRBs) as energy dissipating boundary elements in the first story. The only elements designed to dissipate energy in the inelastic range are the BRBs. The building specimen achieved low-structural damage and enhanced-performance goals, being able to reach a 4% roof drift ratio with little loss of strength and stiffness. The proposed pivoting detail was effective in mitigating compressive damage at the wall toe. To support the experimental campaign and future design procedures, a high-fidelity numerical model of the building was developed using OpenSees.

**KEYWORDS:** buckling-restrained braces, experimental testing, mass timber, numerical model, pivoting spine

## 1 INTRODUCTION

The emergence of mass timber as a novel construction material poses new opportunities for the development of innovative seismic force-resisting systems that are designed for enhanced-performance goals beyond the scope of prescriptive codes [1]. For example, mass timber walls can be designed as structural spines. A spine is a stiff and strong vertical element or portion of the structure that is designed to remain essentially elastic in every vibrational mode, thereby imposing a more uniform drift distribution with building height [2], [3], mitigating story mechanisms [4], [5], and enabling the designer to bypass potential geometric or mass irregularities [6]. If detailed properly and combined with supplemental energy dissipators, mass timber spines are capable of deforming well into the inelastic range during strong ground shaking with stable energy dissipation and, in some cases, low-damage seismic performance [7]–[19].

Despite efforts to standardize mass timber wall design in the United States [20]–[23], alternative means and methods, e.g. performance-based design methods [24]–[28], are often needed to design systems employing mass timber spines, since mass timber seismic force-resisting systems frequently fall outside prescriptive clauses [29]–[32]. However, such methods rely on numerical models grounded on extensive experimental data and can be computationally expensive, thereby limiting the design of mass timber spines in practice. Consequently, experimental testing and numerical validation are necessary to support the development of more practical design methods that better reflect the existing seismic design philosophy in the U.S. to facilitate the use of mass timber systems, including those with spines.

This research contributes to existing experimental data through full-scale quasi-static cyclic testing of a three-story mass timber building featuring a seismic force-resisting system employing a Mass Ply Panel (MPP) pivoting spine with vertically-oriented unbonded steel buckling-restrained braces (BRBs). The specimen was tested in October 2022 at the A.A. Red Emmerson Advanced Wood Products Laboratory at Oregon State University as part of ongoing research on low-damage mass timber seismic force-resisting systems. A numerical model was developed to support the experimental campaign and aid in the development and validation of future design procedures.

[1] Gustavo A. Araujo R., Stanford University, Stanford, CA, USA, garaujor@stanford.edu
[2] Barbara G. Simpson, Stanford University, Stanford, CA, USA, bsimpson@stanford.edu
[3] Tu X. Ho, Oregon State University, Corvallis, OR, USA, tu.ho@oregonstate.edu
[4] Gustavo F. Orozco O., Oregon State University, Corvallis, OR, USA, gustavo.orozco@oregonstate.edu
[5] Andre R. Barbosa, Oregon State University, Corvallis, OR, USA, andre.barbosa@oregonstate.edu
[6] Arijit Sinha, Oregon State University, Corvallis, OR, USA, arijit.sinha@oregonstate.edu

https://doi.org/10.52202/069179-0286

## 2 EXPERIMENTAL PROGRAM

### 2.1 TEST SPECIMEN

The test specimen consisted of a two-bay by two-bay three-story building segment selected from a case-study building archetype; see Figure 1 through Figure 3. The building segment had a square floor plan with an area of approximately 12.2 m x 12.2 m = 149 m$^2$ (1,600 ft$^2$). The first story was slightly taller than the others, with a height of 3.15 m (10.3 ft); the remaining stories had a typical story height of 2.75 m (9 ft).

The gravity system featured four frames made of simply-supported laminated-veneer lumber (LVL) beams and LVL columns. Beams and columns were connected using customized Simpson Strong-Tie column caps with vertically-slotted holes at the column ends to allow for rocking at the beam-to-column interface with minimal moment restraint, effectively accommodating large story drift demands [16]. The gravity connections were braced against lateral-torsional buckling using a L-shaped cross-section steel members. Diaphragm panels were also MPP supported by the LVL beams.

The building specimen was subjected to two separate phases of experimental testing. Phase 1, which is the object of this paper, featured an MPP wall designed as a pivoting spine, supplemented by two-vertically oriented BRBs attached to the wall boundaries in the first-story; see Figure 2(a). The spine is located between two collar beams. In comparison to a rocking wall, the proposed pivoting wall does not impact the foundation during shaking, which alleviates potential crushing at the toe at the base of the wall [33], [34], which might render repairs impractical. Other methods of mitigating crushing at the wall toe have also been proposed [8]. Uplift at the base is restrained by two steel threaded rods connected to a steel plate screwed to the MPP wall at both sides and the external energy dissipators. The base shear is transferred from the spine to the foundation through cross-ply bearing of the MPP on two stiff shear key plates located at the edges of the wall panel. The proposed seismic force-resisting system takes inspiration from previous research on pin-supported reinforced concrete walls [35]–[41] and steel braced frames [42]–[45].

The BRBs are bolted at both ends to gusset plates. The top gusset plate is ultimately connected to the MPP wall through steel side plates and 45-deg inclined, fully threaded screws; see Figure 2(b). The design detail takes advantage of the high strength and stiffness of inclined screws in tension [46], [47], while compressive forces are transferred through bearing of the MPP on top of the timber-to-BRB connection.

To ensure torsional stability of the building specimen during unidirectional cyclic testing, a series of platform-construction MPP walls, termed herein out-of-plane walls, were installed around the perimeter of the building in the perpendicular-to-loading direction. The out-of-plane walls were connected to the MPP floors using standard angle brackets [22] designed to resist 10% of the expected in-plane capacity of the spine.

General dimensions and material properties of the different elements in the specimen are shown in Table 1.

***Table 1**. General dimensions and material properties.*

| Element | Material | Dimensions |
|---|---|---|
| Floor panels | Freres F16-7 MPP | 181 mm thick |
| Columns | Boise Cascade Douglas-fir LVL | 178 mm × 178 mm cross section |
| Beams | Boise Cascade Douglas-fir LVL | 133 mm × 559 mm cross section |
| Spines | Freres F16-8 MPP | 207 mm thick |
| BRBs | CoreBrace bolted brace | $A$ = 1,290 mm$^2$<br>$L_{core}$ = 2.03 m<br>$L_{brace}$ = 3.05 m |
| Foundation beams (spine and gravity system) | ASTM A992 | W12×136 [in×plf] |
| | Boise Cascade Douglas-fir LVL | 178 mm × 356 mm cross section |
| Beam-to-column connections | Simpson Strong-tie column cap | Customized to project |

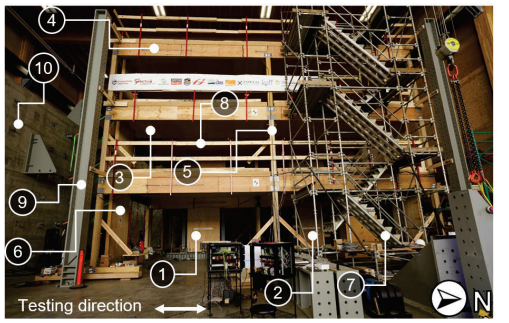


1 Pivoting MPP spine with BRBs (Phase 1)
2 Rocking MPP spine with UFPs (Phase 2)
3 MPP diaphragm
4 LVL beam
5 LVL column
6 Platform-construction MPP walls for torsional stability
7 Scaffolding
8 Guardrail
9 Test-setup steel column
10 Reaction concrete wall

***Figure 1:** Three-story building specimen.*


https://doi.org/10.52202/069179-0286

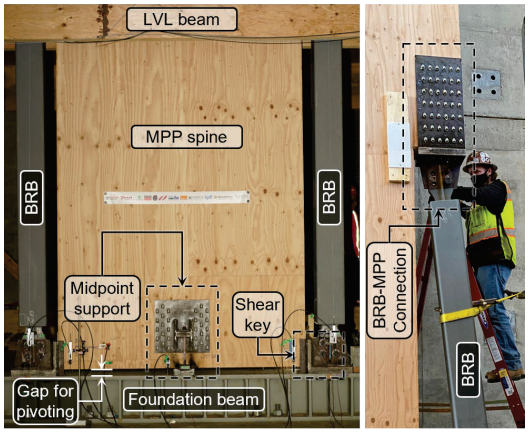


(a) (b)

***Figure 2:*** *Pivoting MPP spine specimen: (a) first-story components and (b) BRB-MPP screwed connection.*

## 2.2 SEISMIC DESIGN

The building was assumed to be representative of an office building archetype located in Seattle, WA, USA (47.58227 N, 122.33111 W). The building specimen was designed following traditional prescriptive seismic design principles from ASCE 7-16 [48], with additional stiffness and strength considerations to include enhanced-performance goals under multiple hazard levels, including seismic demands associated with the Risk-Targeted Maximum Considered Earthquake ($MCE_R$), in addition to the Design Earthquake (DE). The design method was broken into three major components: (i) design of the BRBs, (ii) design of the spine, and (iii) design of the diaphragm and connection details.

The BRBs were designed to resist the entirety of the overturning moment resulting from the design lateral forces, which were obtained using $R = 8$, consistent with the design of buckling-restrained braced-frames. This value of $R$ will be validated in the future. The yield length of the BRB was selected to keep strain demands in the core at the $MCE_R$ level below 2.5% to mitigate fracture due to low-cycle fatigue and $10\varepsilon_y$ (where $\varepsilon_y$ is the yield strain) to target Life Safety per ASCE 41-17 [49].

The spine was proportioned to limit inelastic story drift ratios to 2.0% at the DE level following a displacement-based design approach [49], [50]. In this approach, an equivalent single-degree-of-freedom system is used to estimate the maximum-allowed structural period of the system based on the demands from the DE spectrum. In addition, the MPP spine was designed to remain elastic up to 4.0% roof drift ratio under a first-mode loading pattern to target enhanced performance beyond the $MCE_R$. Design forces were derived from the expected inelastic forces delivered by the BRBs to the spine at a 4.0% roof drift ratio and the near-elastic demands expected in the higher modes. The seismic design of the spine and the BRBs are covered in detail in ref. [51].

Diaphragms and their components, including splines, coiled straps, collectors, and the shear transfer mechanism, were preliminary designed using the alternative design method from ASCE 7-16 §12.10.3, with timber and fastener strength per NDS 2018 [52] and manufacturer recommendations, respectively. The design was then adjusted for the estimated capacity of the spine at a 4% roof drift ratio. More details on the design and expected performance of the diaphragms can be found in refs. [53], [54].

## 2.3 TEST SETUP AND INSTRUMENTATION

Lateral cyclic loads were applied to the structure at each floor level using three actuators, one per level, connected through stiff reaction steel beams to an L-shaped, 7.70-m (25.25-ft) tall reaction wall; see Figure 3. The concentrated load from the actuators was distributed across the MPP diaphragm panels using an assembly of load-transfer steel beams at the south side of the building and LVL beams spanning along the north-south direction. The LVL beams are connected to the MPP diaphragm using screwed steel angle plates and brackets.

The instrumentation layout was designed to measure the global load-displacement behaviour of the system and the local deformations in the spine, BRBs, diaphragm panels and connections. Applied loads at each level were recorded using the corresponding actuator load cells. Lateral displacements of the system in the direction of loading were determined using string potentiometers connected to fixed points in the perimeter of the laboratory. LVDTs were used to measure the tilting behaviour of the MPP spine at the base and the axial deformation of the BRBs. Strain gauges were installed in the elastic regions of each BRB and in the pivot-support rods to estimate axial forces in these elements.

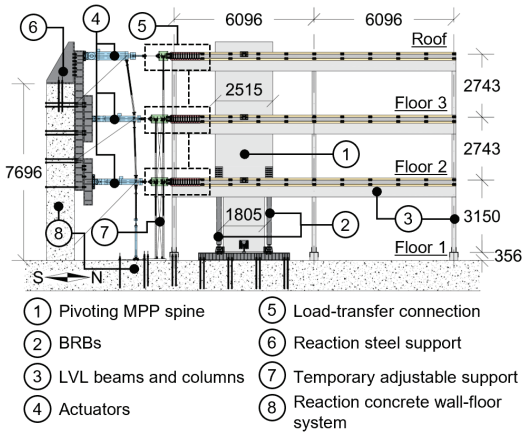


***Figure 3:*** *Test setup. Units: mm.*

## 2.4 LOADING PROTOCOL

The specimen was subjected to two types of loading protocols:

(i) **First mode:** a quasi-static cyclic loading procedure derived from CUREE [55] to assess the behaviour of the spine subjected to a first-mode loading distribution up to 4% roof drift ratio, which was the displacement demand targeted in the design for enhanced performance; see Figure 4 and Figure 5(a).

https://doi.org/10.52202/069179-0286

(ii) **"Higher mode":** a quasi-static half-cycle procedure following a "higher-mode"-like loading distribution up to a base shear of 178 kN (40 kip) to verify the spine remained elastic in the higher modes; see Figure 5(b). The load distribution was selected to satisfy modal orthogonality assuming uniform mass distribution.

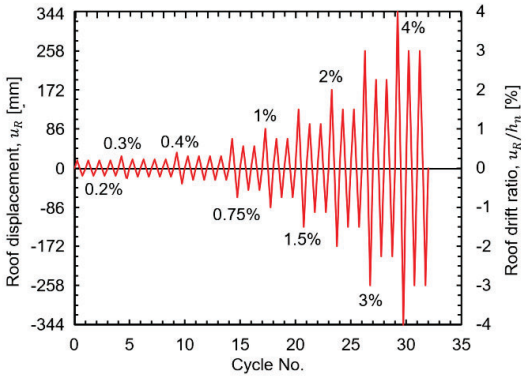


***Figure 4:*** *First-mode displacement protocol with primary-cycle amplitudes labelled.*

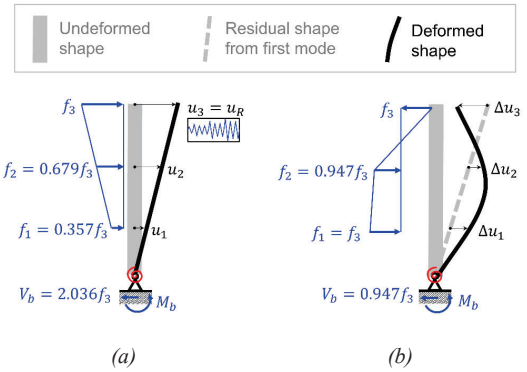


(a) (b)

***Figure 5:*** *Testing load distributions: (a) first mode and (b) "higher mode".*

# 3 EXPERIMENTAL RESULTS

## 3.1 GLOBAL FIRST-MODE BEHAVIOUR

Figure 6 shows the global base shear-roof displacement hysteretic behaviour of the building specimen when subjected to a first-mode loading distribution; Figure 7 breaks down the experimental results by primary and trailing cycles of different peak cyclic amplitudes. The specimen performed as intended, maintaining a nearly uniform distribution of lateral drifts across all stories for the entire loading protocol; see Figure 8. The building exhibited a full and stable global hysteretic behaviour, including a complete cycle at the target enhanced-performance drift of $\theta = 4.0\%$ and two subsequent cycles at $\theta = 3.0\%$, without observed loss of lateral strength. In general, the behavior of the system was comparable to the observed in previous tests on steel and concrete pivoting spines supplemented by BRBs [33], [44].

Observed residual drifts significantly increased after yielding of the BRBs due to the absence of a self-centering mechanism in the structure and accumulated residual deformations in the BRBs. After the cycles to $\theta = 2.0\%$ (the target drift at the DE level), the observed residual roof drift ratio was 1.38%. Similarly, the residual drifts after the cycles to $\theta = 3.0\%$ and 4.0% were 2.3% and 3.3%, respectively. Such level of residual drift may result in increased repair costs and downtime after an earthquake event. A plausible solution for this issue would be the use of self-centering BRBs [56]–[58], post-tensioning or other similar devices.

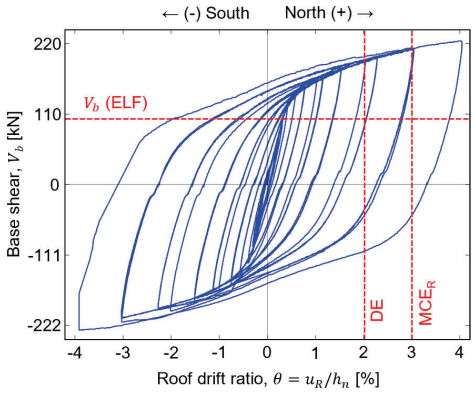


***Figure 6:*** *Global hysteretic behaviour of the specimen subjected a first-mode loading distribution.*

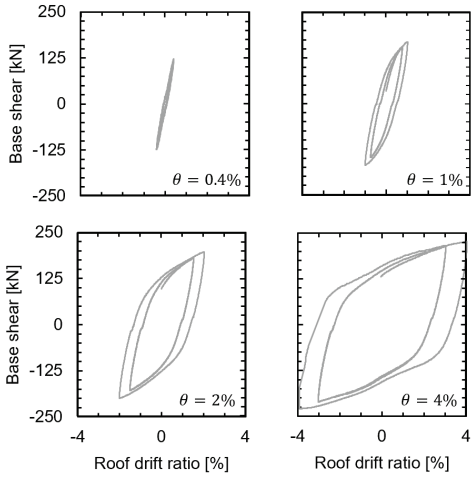


***Figure 7:*** *Global hysteretic loops at 0.4%, 1%, 2%, and 4% primary cycles, and subsequent trailing cycles.*


https://doi.org/10.52202/069179-0286

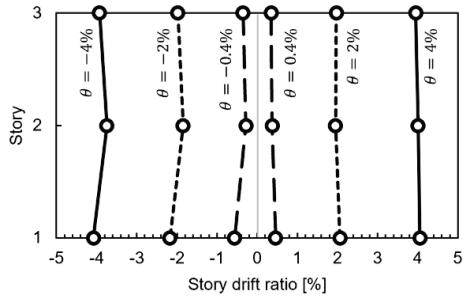


***Figure 8:*** *Story drift profiles at different roof drift levels θ.*

### 3.2 BRB BEHAVIOUR

Damage investigation after the primary cycles and post-processed instrumentation data were used to assess the behaviour of each of the components of the test specimen, including the BRBs, the MPP spine and connections, MPP diaphragms and the gravity system.

Inelastic behaviour was observed in the BRBs at low drift levels ($\theta > 0.40\%$). After yielding, the BRBs started to exhibit significant residual elongation or shortening of the yielding core when unloaded in tension or compression, respectively. Figure 9(a) shows photographical evidence of the state of the BRBs before testing and after completion of the loading procedure. The BRBs were able to sustain the axial deformation demands imposed by the tilting mode of the spine without fracture or the core or instabilities at the connection regions. Due to inelastic deformations in the BRBs, the BRB-MPP spine system remained tilted towards the south direction at the end of the test, resulting in a residual roof drift ratio of 3.2% after the last cycle; see Figure 9(b).

Both BRBs exhibited similar axial deformations in tension and compression, as shown in Figure 10(a), due to the rod preventing uplift at the pivot support. By vertical equilibrium, without the addition of the rod detail, the wall would have uplifted at the middle and the deformation demands in the BRBs would have been greater in tension than in compression. Deformation demands in the BRBs at the cycles up to $\theta = 4\%$ were in the order of 40 mm (1.57 in), resulting in strains of nearly 2% in the yielding core.

Figure 10(b) presents the estimated hysteretic axial force-deformation behaviour of the BRBs. Axial forces were estimated using the average of the data recorded by four strain gauges installed near the ends of the BRBs, while axial deformations were measured using LVDTs oriented lengthwise on either side of the BRB (assuming deformations occurred primarily in the yielding region of the core). The strain gauges installed in the transition region were expected to remain elastic. In the test, however, flaking at the BRB end connections was observed during damage inspections after the 3.0% cycles, and this strain gage data is suspect. For this reason, the estimated hysteretic behaviour shown in Figure 10(b) is separated into cycles before and after 2.0%. The recorded data suggest that the BRBs exhibited kinematic and isotropic strain hardening after yielding, which is consistent with previous observations on systems employing BRBs [44], [47], [59]–[65]. However, the effects of isotropic hardening were not evident in the observed global behaviour of the system. It is suspected that other sources of softening in the system could have overshadowed the effect of isotropic hardening in the system.

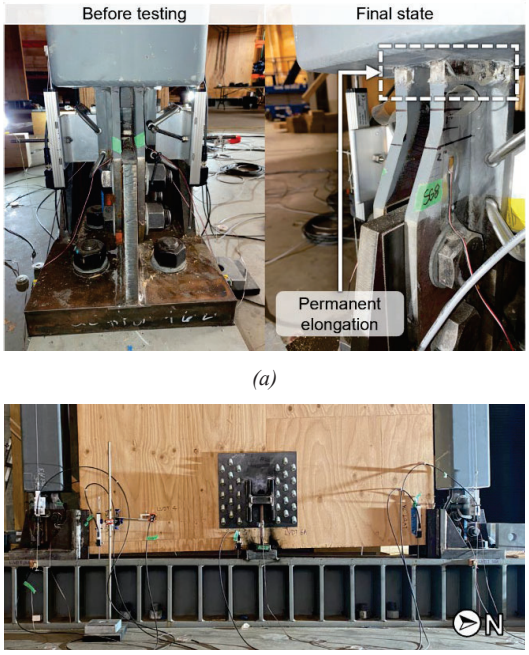


*(a)*

*(b)*

***Figure 9:*** *Damage investigation in the BRBs: (a) permanent elongation of the yielding core at the bottom, near the foundation, and (b) permanent tilting mode after the test due to inelastic deformations in the BRBs.*

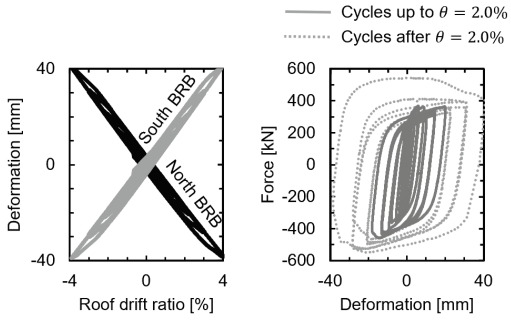


*(a)* *(b)*

***Figure 10:*** *Experimentally-observed behaviour of BRBs:(a) axial deformation vs roof drift ratio for both BRBs and (b) hysteretic force-displacement behaviour.*

### 3.3 MPP SPINE AND CONNECTIONS

The MPP spine remained essentially elastic throughout the entire testing protocol. The midpoint pivot support behaved as intended, limiting uplift due to the unbalance force between the two BRBs acting in tension and compression (i.e., by vertical equilibrium). Small southward sliding of the MPP spine with respect to the

foundation was observed from low-amplitude cycles; see Figure 11(a).

Minimal, cosmetic damage was observed in the spine at the location of the base shear keys, as shown in Figure 11(b). The observed damage was attributed to a combination of bearing stresses in the cross-ply direction of the MPP and friction between the steel and the outer MPP plies in the vertical direction.

No visible damage was observed in the MPP spine above the first floor. The BRB-to-MPP connections did not show any signs of slip of the steel plates or splitting/crushing in the MPP boundaries at the screwed connections.

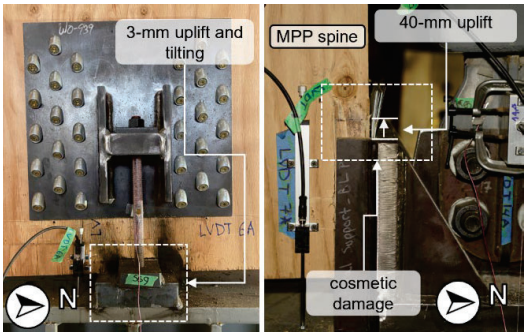


(a) (b)

***Figure 11:*** *Damage observation in the MPP spine after the test: (a) midpoint pivot support, and (b) north base-shear key.*

### 3.4 DIAPHRAGMS AND GRAVITY SYSTEM

The MPP diaphragms remained essentially elastic throughout the entire test. No visible signs of slip in the plywood splines or openings between the diaphragm panels was observed. Similarly, the beam-to-column connections in the gravity system were able to accommodate story drift demands up to $\theta = 4.0\%$ through rocking, without inducing visible damage to the LVL columns.

### 3.5 GLOBAL HIGHER-MODE BEHAVIOUR

Figure 12 summarizes the global behaviour of the building when subjected to the "higher-mode"-like loading distribution. The testing procedure started after the full first-mode loading protocol was applied, with the building tilting southwards with a residual drift of $\theta = -2.25\%$. The specimen behaved near-elastic, as is intended for the spine design, under the higher-mode loads. The load-displacement relation reached the maximum targeted base shear in a near-linear way, with high stiffness and little increase in lateral displacements; see Figure 12(a-b). Under this force distribution, the behaviour of the spine resembled that of a simply-supported deep beam under a four-point loading distribution, as shown by the incremental displacement profile in Figure 12(b). No visible damage in the connections or MPP spine was observed at the end of the test. Deformation and force demands in the BRBs did not vary significantly throughout the "higher-mode"-like testing procedure.

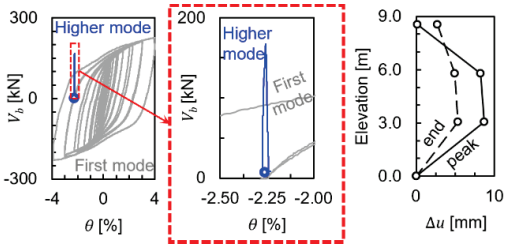


(a) (b)

***Figure 12:*** *"Higher-mode" behaviour of the building: (a) Base shear vs. roof drift ratio; (b) Incremental displacements relative to the first-mode residual deformed shape at peak base shear and at the end of the test.*

## 4 NUMERICAL VALIDATION

### 4.1 MODELING SCHEME

The cyclic behaviour of the test specimen was estimated using a two-dimensional nonlinear numerical model in OpenSees [66], as shown in Figure 13. The numerical model included the LVL beams and columns, pivoting MPP spine, BRBs, and foundation beam for the spine. The BRB-to-spine, diaphragm-to-spine, and foundation connections were also modelled. Material properties were based on existing test data at the component level [44], [62], [67]–[69]. More details on the numerical model can be found in ref. [51], [70].

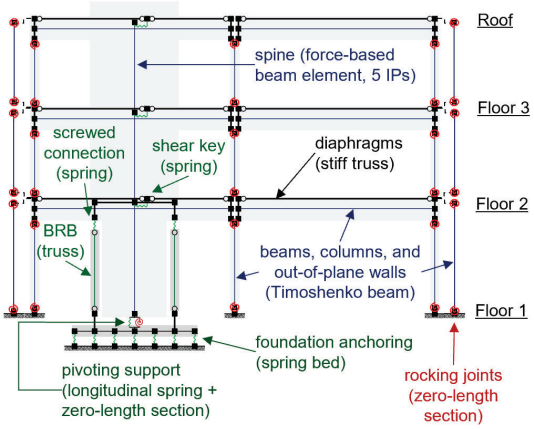


***Figure 13:*** *Two-dimensional numerical model of the building specimen.*

### 4.2 SIMULATED BEHAVIOUR.

Figure 13 compares the experimentally-measured cyclic behaviour of the building specimen and the BRBs under a first-mode loading distribution against the numerical estimates. At the system level, the simulation results agree well with the observed behaviour of the specimen; see Figure 13(a). At the BRB level, the simulation approximates the experimentally-measured behaviour for cycles up to $\theta = 2.0\%$. For larger values of $\theta$, the simulation significantly diverges from the BRB experimental data, particularly on the tension side. It should be noted that this discrepancy is likely due to the strain gage data used to estimate the axial force in the


https://doi.org/10.52202/069179-0286

BRBs becoming corrupted after $\theta = 2.0\%$. In general terms, the proposed numerical model estimates well the behaviour of the specimen and is suitable for extensive numerical analyses typical in performance and collapse assessment.

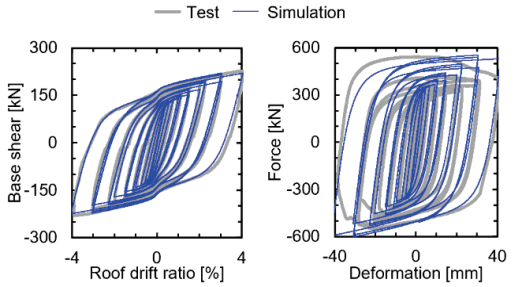


***Figure 14:*** *Experimentally-measured vs simulated behaviour: (a) system level and (b) BRBs.*

## 5 CONCLUSIONS

This study introduced a seismic force-resisting system employing a mass timber pivoting spine supplemented by BRBs as energy dissipators. The behaviour of the system was studied through experimental quasi-static cyclic testing of a three-story full-scale building specimen and numerical modelling. The study illustrates that mass timber walls can be effectively designed as structural spines with the addition of BRBs as energy dissipators. The specimen achieved low-structural damage and enhanced-performance goals. The proposed pivoting detail was effective in mitigating compressive damage at the wall toe. The behaviour of the system was significantly influenced by the inelastic and strain-hardening behaviour of the BRBs, resulting in high residual drifts due to the absence of self-centering mechanisms.

These findings can be useful for improving the design and evaluation of mass timber structures in future studies. Future work should explore the addition of self-centering devices that help to reduce residual drifts and assess the seismic performance of the system through nonlinear dynamic analysis.

## ACKNOWLEDGEMENTS

The authors would like to thank graduate students Steven Kontra, Patricio Uarac, and undergraduate students Kristian Walker, and Tanner Field for their help with instrumentation and testing. In addition, the authors would like to thank the laboratory technicians Byrne Miyamoto, Phil Mann, and Mark Gerig of the Tallwood Design Institute for their support throughout the experimental program.

This project was executed under the USDA Agricultural Research Service Award No. 58-0204-9-165. Part of the work was also supported by the National Science Foundation under awards #2120683, #2120692, and #2120684. Special thanks to our industry partners, KPFF, Holmes, Fortis Construction, Carpenters Union, CoreBrace, Boise Cascade, Simpson Strong-Tie, and Freres Engineered Wood, for supporting this experimental program. The findings, opinions, recommendations, and conclusions in this paper are those of the authors and do not necessarily reflect the views of others, including the sponsors.

## REFERENCES

[1] S. Pei, J. D. Dolan, R. B. Zimmerman, E. McDonnell, P. Line, and M. Popovski, "From Testing to Codification: Post-tensioned Cross Laminated Timber Rocking Walls," in *International Network for Timber Engineering Research (INTER)*, 2019.

[2] B. Alavi and H. Krawinkler, "Strengthening of moment-resisting frame structures against near-fault ground motion effects," *Earthq Eng Struct Dyn*, vol. 33, no. 6, pp. 707–722, 2004, doi: https://doi.org/10.1002/eqe.370.

[3] Z. Qu, L. Ye, and A. Wada, "Seismic Damage Mechanism Control of RC Ductile Frames from a Stiffness Point of View," in *8th International Conference on Urban Earthquake Engineering*, 2011. [Online]. Available: http://qu-zhe.net/Resource/Struct/CUEE8-QuZ.pdf

[4] D. Mar, "Design Examples using Mode Shaping Spines for Frame and Wall Buildings," in *9th U.S. National and 10th Canadian Conference on Earthquake Engineering*, 2010.

[5] L. Panian, N. Bucci, and B. Janhunen, "BRBM Frames: An Improved Approach to Seismic-Resistant Design Using Buckling-Restrained Braces," in *Improving the Seismic Performance of Existing Buildings and Other Structures 2015*, 2015, pp. 632–643. doi: doi:10.1061/9780784479728.052.

[6] J. Osteraas, J. Hunt, and G. Luth, "Performance Based Seismic Design of the Gigafactory in Tesla Time," in *2017 SEAOC Convention*, 2017. [Online]. Available: https://cdn.ymaws.com/www.seaoc.org/resource/resmgr/Convention_Proceedings/2017/009_PAPER_Osteraas.pdf

[7] T. Akbas *et al.*, "Analytical and Experimental Lateral-Load Response of Self-Centering Posttensioned CLT Walls," *Journal of Structural Engineering*, vol. 143, no. 6, p. 4017019, 2017, doi: doi:10.1061/(ASCE)ST.1943-541X.0001733.

[8] H.-E. Blomgren *et al.*, "Full-Scale Shake Table Testing of Cross-Laminated Timber Rocking Shear Walls with Replaceable Components," *Journal of Structural Engineering*, vol. 145, no. 10, p. 4019115, 2019, doi: doi:10.1061/(ASCE)ST.1943-541X.0002388.

[9] Z. Chen, M. Popovski, and A. Iqbal, "Structural Performance of Post-Tensioned CLT Shear Walls with Energy Dissipators," *Journal of Structural*

*Engineering*, vol. 146, no. 4, p. 4020035, 2020, doi: 10.1061/(asce)st.1943-541x.0002569.

[10] D. Fitzgerald, T. H. Miller, A. Sinha, and J. A. Nairn, "Cross-laminated timber rocking walls with slip-friction connections," *Eng Struct*, vol. 220, p. 110973, 2020, doi: https://doi.org/10.1016/j.engstruct.2020.110973.

[11] A. Hashemi and P. Quenneville, "Large-scale testing of low damage rocking Cross Laminated Timber (CLT) wall panels with friction dampers," *Eng Struct*, vol. 206, p. 110166, 2020, doi: https://doi.org/10.1016/j.engstruct.2020.110166.

[12] A. Iqbal, T. Smith, S. Pampanin, M. Fragiacomo, A. Palermo, and A. H. Buchanan, "Experimental Performance and Structural Analysis of Plywood-Coupled LVL Walls," *Journal of Structural Engineering*, vol. 142, no. 2, p. 4015123, 2016, doi: doi:10.1061/(ASCE)ST.1943-541X.0001383.

[13] M. Massari, M. Savoia, and A. R. Barbosa, "Experimental and Numerical Study of Two-Story Post-Tensioned Seismic Resisting CLT Wall with External Hysteretic Energy Dissipaters," in *Atti del XVII Convegno ANIDIS L'ingegneria Sismica in Italia : Pistoia, 17-21 settembre 2017. - ( Studi in tema di internet ecosystem)*, Pisa: Pisa University Press, 2017. [Online]. Available: http://digital.casalini.it/4215425

[14] M. P. Newcombe, "Seismic design of post-tensioned timber frame and wall buildings," Christchurch, New Zealand, 2011.

[15] A. Palermo, S. Pampanin, M. Fragiacomo, A. H. Buchanan, and B. L. Deam, "Innovative seismic solutions for multi-storey LVL timber buildings," *9th World Conference on Timber Engineering, WCTE 2006*. Portland, OR, 2006.

[16] S. Pei *et al.*, "Experimental Seismic Response of a Resilient 2-Story Mass-Timber Building with Post-Tensioned Rocking Walls," *Journal of Structural Engineering*, vol. 145, no. 11, p. 4019120, 2019, doi: doi:10.1061/(ASCE)ST.1943-541X.0002382.

[17] F. Sarti, A. Palermo, and S. Pampanin, "Quasi-Static Cyclic Testing of Two-Thirds Scale Unbonded Posttensioned Rocking Dissipative Timber Walls," *Journal of Structural Engineering*, vol. 142, no. 4, p. E4015005, 2016, doi: doi:10.1061/(ASCE)ST.1943-541X.0001291.

[18] F. Sarti, A. Palermo, and S. Pampanin, "Development and Testing of an Alternative Dissipative Posttensioned Rocking Timber Wall with Boundary Columns," *Journal of Structural Engineering*, vol. 142, no. 4, p. E4015011, 2016, doi: doi:10.1061/(ASCE)ST.1943-541X.0001390.

[19] R. Soti, A. Sinha, I. Morrell, and B. T. Miyamoto, "Response of self-centering mass plywood panel shear walls," *Wood and Fiber Science*, vol. 52, no. 1, pp. 102–116, 2020.

[20] ASCE 7, "Minimum Design Loads and Associated Criteria for Buildings and Other Structures (ASCE/SEI 7-22)." American Society of Civil Engineers, Reston, VA, 2022.

[21] AWC, "SDPWS - Special Design Provisions for Wind and Seismic with Commentary," vol. ANSI/AWC SDPWS. American Wood Council, Leesburg, VA, 2021.

[22] FEMA P-2082-1 and Federal Emergency Management Agency, "NEHRP Recommended Seismic Provisions for New Buildings and Other Structures," Federal Emergency Management Agency, Washington, D.C., 2020.

[23] IBC, "2021 International Building Code." International Code Council, Inc., USA, 2020.

[24] G. G. Deierlein, H. Krawinkler, and C. A. Cornell, "A framework for performance-based earthquake engineering," *2003 Pacific Conference on Earthquake Engineering*. New Zealand Society for Earthquake Engineering, Christchurch, New Zealand, 2003. [Online]. Available: https://www.nzsee.org.nz/db/2003/View/Paper140s.pdf

[25] FEMA P-58-6, "Guidelines for Performance-Based Seismic Design of Buildings." Federal Emergency Management Agency, Washington, D.C., 2018.

[26] S. Günay and K. M. Mosalam, "PEER Performance-Based Earthquake Engineering Methodology, Revisited," *Journal of Earthquake Engineering*, vol. 17, no. 6, pp. 829–858, 2013, doi: 10.1080/13632469.2013.787377.

[27] H. Krawinkler and E. Miranda, "Performance-Based Earthquake Engineering," in *Earthquake Engineering: From Engineering Seismology to Performance-Based Engineering*, 1st Edition., Y. Bozorgnia and V. v Bertero, Eds. Boca Raton, FL: CRC Press, 2004. doi: https://doi.org/10.1201/9780203486245.

[28] J. P. Moehle and G. G. Deierlein, "A Framework Methodology for Performance-Based Earthquake Engineering," *13th World Conference on Earthquake Engineering*. Vancouver, Canada, 2004. [Online]. Available: https://www.iitk.ac.in/nicee/wcee/article/13_679.pdf

[29] E. McDonnell and B. Jones, "Performance-Based Engineering Provides Path to More Compelling Mass Timber Projects," *Technology|Architecture + Design*, vol. 4, no. 1, pp. 9–13, 2020, doi: 10.1080/24751448.2020.1705709.

[30] B. T. Teweldebrhan and S. Tesfamariam, "Performance-based design of tall-coupled cross-laminated timber wall building," *Earthq Eng*


https://doi.org/10.52202/069179-0286

*Struct Dyn*, vol. 51, no. 7, pp. 1677–1696, 2022, doi: https://doi.org/10.1002/eqe.3633.

[31] R. B. Zimmerman, H.-E. Blomgren, J. McCutcheon, and A. Sinha, "Catalyst - A Mass Timber Core Wall Building with High Ductility Hold-Downs in a Seismic Region," *2020 World Conference on Timber Engineering*. Santiago, Chile, 2020.

[32] R. B. Zimmerman and E. McDonnell, "Framework - A tall re-centering mass timber building in the United States," *2017 NZSEE Conference*. Wellington, New Zealand, 2017. [Online]. Available: http://db.nzsee.org.nz/2017/O5C.3_Zimmerman_&_McDonnell.pdf

[33] Q. Jiang *et al.*, "Experimental study and numerical simulation of a reinforced concrete hinged wall with BRBs at the base," *Journal of Building Engineering*, vol. 49, p. 104030, 2022, doi: https://doi.org/10.1016/j.jobe.2022.104030.

[34] Q. Jiang *et al.*, "Analysis and experimental testing of a self-centering controlled rocking wall with buckling-restrained braces at base," *Eng Struct*, vol. 269, p. 114843, 2022, doi: https://doi.org/10.1016/j.engstruct.2022.114843.

[35] B. Janhunen, S. Tipping, and J. Wolfe, "Seismic Retrofit of a 1960s Steel Moment-Frame Highrise Using a Pivoting Spine," in *SEAOC 2013 Convention*, 2013. [Online]. Available: https://www.tippingstructural.com/firm/publications

[36] Q. Jiang *et al.*, "Experimental study and numerical simulation of a reinforced concrete hinged wall with BRBs at the base," *Journal of Building Engineering*, vol. 49, p. 104030, May 2022, doi: 10.1016/J.JOBE.2022.104030.

[37] Z. Qu, A. Wada, S. Motoyui, H. Sakata, and S. Kishiki, "Pin-supported walls for enhancing the seismic performance of building structures," *Earthq Eng Struct Dyn*, vol. 41, no. 14, pp. 2075–2091, 2012, doi: https://doi.org/10.1002/eqe.2175.

[38] T. Sun, Y. C. Kurama, and J. Ou, "Practical displacement-based seismic design approach for PWF structures with supplemental yielding dissipators," *Eng Struct*, vol. 172, pp. 538–553, 2018, doi: https://doi.org/10.1016/j.engstruct.2018.05.120.

[39] A. Wada, Z. Qu, H. Ito, S. Motoyui, H. Sakata, and K. Kasai, "Seismic Retrofit Using Rocking Walls and Steel Dampers," in *Improving the Seismic Performance of Existing Buildings and Other Structures*, 2009, pp. 1010–1021. doi: doi:10.1061/41084(364)92.

[40] A. Wada, Z. Qu, S. Motoyui, and H. Sakata, "Seismic retrofit of existing SRC frames using rocking walls and steel dampers," *Frontiers of Architecture and Civil Engineering in China*, vol. 5, no. 3, p. 259, 2011, doi: 10.1007/s11709-011-0114-x.

[41] X. Wang, T. Wang, and Z. Qu, "An experimental study of a damage-controllable plastic-hinge-supported wall structure," *Earthq Eng Struct Dyn*, vol. 47, no. 3, pp. 594–612, 2018, doi: https://doi.org/10.1002/eqe.2981.

[42] X. Chen, T. Takeuchi, and R. Matsui, "Simplified design procedure for controlled spine frames with energy-dissipating members," *J Constr Steel Res*, vol. 135, pp. 242–252, 2017, doi: https://doi.org/10.1016/j.jcsr.2017.04.017.

[43] L. Gioiella, E. Tubaldi, F. Gara, L. Dezi, and A. Dall'Asta, "Modal properties and seismic behaviour of buildings equipped with external dissipative pinned rocking braced frames," *Eng Struct*, vol. 172, pp. 807–819, 2018, doi: https://doi.org/10.1016/j.engstruct.2018.06.043.

[44] B. G. Simpson and S. A. Mahin, "Experimental and Numerical Investigation of Strongback Braced Frame System to Mitigate Weak Story Behavior," *Journal of Structural Engineering*, vol. 144, no. 2, p. 4017211, 2018, doi: doi:10.1061/(ASCE)ST.1943-541X.0001960.

[45] T. Takeuchi, X. Chen, and R. Matsui, "Seismic performance of controlled spine frames with energy-dissipating members," *J Constr Steel Res*, vol. 114, pp. 51–65, 2015, doi: https://doi.org/10.1016/j.jcsr.2015.07.002.

[46] Z. Chen, M. Popovski, and A. Iqbal, "Structural Performance of Post-Tensioned CLT Shear Walls with Energy Dissipators," *Journal of Structural Engineering*, vol. 146, no. 4, p. 04020035, Jan. 2020, doi: 10.1061/(ASCE)ST.1943-541X.0002569.

[47] W. Dong, M. Li, C. L. Lee, G. MacRae, and A. Abu, "Experimental testing of full-scale glulam frames with buckling restrained braces," *Eng Struct*, vol. 222, p. 111081, Nov. 2020, doi: 10.1016/J.ENGSTRUCT.2020.111081.

[48] ASCE 7, "Minimum Design Loads and Associated Criteria for Buildings and Other Structures (ASCE/SEI 7-16)." American Society of Civil Engineers, Reston, VA, 2016.

[49] ASCE 41, "Seismic Evaluation and Retrofit of Existing Buildings (ASCE/SEI 41-17)." American Society of Civil Engineers, Reston, VA, 2017.

[50] M. Panagiotou and J. I. Restrepo, "Displacement-Based Method of Analysis for Regular Reinforced-Concrete Wall Buildings: Application to a Full-Scale 7-Story Building Slice Tested at UC-San Diego," *Journal of Structural Engineering*, vol. 137, no. 6, pp. 677–690, 2011, doi: doi:10.1061/(ASCE)ST.1943-541X.0000333.

[51] G. A. Araújo R., "Design, Experimental Testing, and Numerical Analysis of a Three-Story Mass

Timber Building with a Pivoting Spine and Buckling-Restrained Energy Dissipators," MS Thesis, Oregon State University, Corvallis, OR, 2022.

[52] AWC, "National Design Specification (NDS) for Wood Construction with Commentary," vol. ANSI/AWC NDS. American Wood Council, Leesburg, VA, 2018.

[53] L. G. Rodrigues, A. R. Barbosa, G. F. Orozco O., J. M. Branco, A. Sinha, and B. G. Simpson, "Analytical model and finite element modeling strategy for the design and assessment of mass timber diaphragms," in *12th National Conference on Earthquake Engineering*, 2022.

[54] G. F. Orozco O., T. X. Ho, G. A. Araújo R., A. R. Barbosa, A. Sinha, and B. G. Simpson, "Innovative Mass Timber Seismic Lateral Force Resisting Systems: Testing of a Full-scale Three-story Building with Mass Ply Panels (MPP) Rocking Walls," in *12th National Conference on Earthquake Engineering*, 2022.

[55] H. Krawinkler, F. Parisi, L. Ibarra, A. Ayoub, and R. Medina, "Development of a Testing Protocol for Woodfram Structures," CUREE - Consortium of Universities for Research in Earthquake Engineering, Richmond, CA, 2001.

[56] H. Dong, X. Du, Q. Han, H. Hao, K. Bi, and X. Wang, "Performance of an innovative self-centering buckling restrained brace for mitigating seismic responses of bridge structures with double-column piers," *Eng Struct*, vol. 148, pp. 47–62, 2017, doi: https://doi.org/10.1016/j.engstruct.2017.06.011.

[57] M. R. Eatherton, L. A. Fahnestock, and D. J. Miller, "Computational study of self-centering buckling-restrained braced frame seismic performance," *Earthq Eng Struct Dyn*, vol. 43, no. 13, pp. 1897–1914, 2014, doi: https://doi.org/10.1002/eqe.2428.

[58] D. J. Miller, L. A. Fahnestock, and M. R. Eatherton, "Development and experimental validation of a nickel–titanium shape memory alloy self-centering buckling-restrained brace," *Eng Struct*, vol. 40, pp. 288–298, 2012, doi: https://doi.org/10.1016/j.engstruct.2012.02.037.

[59] C. J. Black, N. Makris, and I. D. Aiken, "Component Testing, Seismic Evaluation and Characterization of Buckling-Restrained Braces," *Journal of Structural Engineering*, vol. 130, no. 6, pp. 880–894, 2004, doi: doi:10.1061/(ASCE)0733-9445(2004)130:6(880).

[60] V. Budaházy, "Modelling of the Hysteretic Behavior of Buckling Restrained Braces," *Conference of Junior Researchers in Civil Engineering*. Budapest University of Technology and Economics, Budapest, Hungary, pp. 34–41, 2012.

[61] L. A. Fahnestock, J. M. Ricles, and R. Sause, "Experimental Evaluation of a Large-Scale Buckling-Restrained Braced Frame," *Journal of Structural Engineering*, vol. 133, no. 9, pp. 1205–1214, 2007, doi: doi:10.1061/(ASCE)0733-9445(2007)133:9(1205).

[62] S. Merritt, C.-M. Uang, and G. Benzoni, "Subassemblage testing of corebrace buckling-restrained braces," University of California, San Diego, La Jolla, California, 2003.

[63] C. Tong, J. Wu, K. Hua, and L. Xie, "Low-Cycle Fatigue Life Estimation Curve for Buckling-Restrained Braces Based on Cumulative Plastic Deformation," *Journal of Earthquake Engineering*, pp. 1–29, 2020, doi: 10.1080/13632469.2020.1772152.

[64] C.-M. Uang, M. Nakashima, and K.-C. Tsai, "Research and application of buckling-restrained braced frames," *International Journal of Steel Structures*, vol. 4, no. 4, pp. 301–313, 2004.

[65] A. Watanabe, Y. Hitomi, E. Saeki, A. Wada, and M. Fujimoto, "Properties of brace encased in buckling-restraining concrete and steel tube," in *Proceedings of ninth world conference on earthquake engineering*, 1988, vol. 4, pp. 719–724.

[66] F. McKenna, M. H. Scott, and G. L. Fenves, "Nonlinear Finite-Element Analysis Software Architecture Using Object Composition," *Journal of Computing in Civil Engineering*, vol. 24, no. 1, pp. 95–107, 2010, doi: doi:10.1061/(ASCE)CP.1943-5487.0000002.

[67] R. Soti, T. X. Ho, and A. Sinha, "Structural Performance Characterization of Mass Plywood Panels," *Journal of Materials in Civil Engineering*, vol. 33, no. 10, p. 4021275, 2021, doi: doi:10.1061/(ASCE)MT.1943-5533.0003902.

[68] T. X. Ho, A. Arora, and A. Sinha, "In-Plane Shear Properties of Mass Ply Panels in Long-Ply Direction," *Journal of Materials in Civil Engineering*, vol. 34, no. 8, p. 4022170, 2022, doi: doi:10.1061/(ASCE)MT.1943-5533.0004327.

[69] B. G. Simpson and S. Mahin, "Design Development for Steel Strongback Braced Frames to Mitigate Concentrations of Damage," Berkeley, CA, 2018.

[70] G. A. Araújo R, B. Simpson, T. X. Ho, G. F. Orozco O, A. R. Barbosa, and A. Sinha, "Numerical Modelling of a Three-Story Building Using a Hybrid of Mass Timber Walls with Buckling-Restrained Braces," in *Proceedings of the 10th International Conference on Behaviour of Steel Structures in Seismic Areas. STESSA 2022. Lecture Notes in Civil Engineering.*, 2022, vol. 262. doi: 10.1007/978-3-031-03811-2_45.


https://doi.org/10.52202/069179-0286